PHYSICAL REVIEW B VOLUME 40, NUMBER 1 1 JULY 1989

Incommensurate structures in highly ordered complex perovskites $Pb(Co_{1/2}W_{1/2})O_3$ and $Pb(Sc_{1/2}Ta_{1/2})O_3$

C. A. Randall, S. A. Markgraf, and A. S. Bhalla
Materials Research Laboratory, The Pennsylvania State University, University Park, Pennsylvania 16802

K. Baba-Kishi
Department of Physics, University of Essex, Colchester, United Kingdom
(Received 15 February 1989)

A transmission electron microscopy study of two *B*-site order perovskites $Pb(Co_{1/2}W_{1/2})O_3$ and $Pb(Sc_{1/2}Ta_{1/2})O_3$ has revealed evidence for an incommensurate phase within the antiferroelectric and ferroelectric phase, respectively. Direct observations by dark field techniques have revealed discommensurate structures in both $Pb(Sc_{1/2}Ta_{1/2})O_3$ and $Pb(Co_{1/2}W_{1/2})O_3$. A possible "lock-in" transition is found in $Pb(Sc_{1/2}Ta_{1/2})O_3$, but the incommensurate to commensurate transition seems to be dependent on the degree of *B*-site order.

INTRODUCTION

The complex lead-based ferroelectric perovskites $Pb(B_xB'_{1-x})O_3$ have received considerable attention from both industrial and academic institutions. Lead-based perovskites have found application in capacitors,[1] actuators,[2] and pyroelectric detectors.[3]

The dielectric behavior of the complex $Pb(B_xB'_{1-x})O_3$ materials is a result of the underlying chemical distribution of *B*-site cations in the perovskite structure. Setter and Cross demonstrated with $Pb(Sc_{1/2}Ta_{1/2})O_3$ that the distribution of the *B*-site cations Sc and Ta could be tailored by various heat treatments (annealing and quenching).[4] The driving forces for diffusion are dependent on the valence and ionic radii differences between the *B*-site cations. When high occupancy disorder exists between the *B*-site cations, nanoscale chemical and strain gradients results. These gradients prevent the long-range "normal" ferroelectric behavior, and so called superparaelectric relaxor ferroelectrics develop.[5–7] The relaxor materials have polar microregions which form over a wide Curie range, and because of their small size are easily thermally agitated about the various polar directions. These relaxors are characterized by a broad frequency dispersive permittivity-temperature relation. With a highly ordered *B*-site sublattice in a perovskite, the ferroelectric behavior is no longer perturbed by nanoscale inhomogeneities, and "normal" long-range ferroelectric behavior occurs.

The $Pb(Co_{1/2}W_{1/2})O_3$ perovskite composition has a highly ordered *B*-site sublattice. There has been much debate in the literature concerning the nature of the ferroic phase below the transition at 32 °C, be it an antiferroelectric[8,9] or ferroelectric displacive phase transition.[10,11] A recent study of the transition temperatures as a function of hydrostatic pressure strongly suggests that the $Pb(Co_{1/2}W_{1/2})O_3$ has an antiferroelectric nature below T_c. Brixel *et al.*,[12] Tamura,[13] and Filip'ev and Fesenko[14] all have suggested the symmetry to be monoclinic. Tamura, in an x-ray study, noted the existence of an incommensurate phase in $Pb(Co_{1/2}W_{1/2})O_3$ down to 150 K. This article confirms the existence of incommensuration in the $Pb(Co_{1/2}W_{1/2})O_3$ and draws attention to the possibility of a new group of incommensurate antiferroelectrics and ferroelectrics in the highly ordered perovskite family.

EXPERIMENTAL PROCEDURE

$Pb(Sc_{1/2}Ta_{1/2})O_3$ single crystals and ceramics were prepared by the methods described earlier.[12] The $Pb(Co_{1/2}W_{1/2})O_3$ was made in ceramic form starting with analytical grade powders, and using a sintering procedure as described by Tomashpol'skii and Venevtsev.[15]

The TEM study was made on ion-beam thinned sections of $Pb(Sc_{1/2}Ta_{1/2})O_3$ and $Pb(Co_{1/2}W_{1/2})O_3$ using a Philips 420. The low-temperature studies were made using a Gatan liquid-nitrogen-cooled stage.

RESULTS

$Pb(Co_{1/2}W_{1/2})O_3$ has an assumed paraelectric to antiferroelectric phase transition at $\approx 32\,^{\circ}C$.[9,10] Cooling below the Curie temperature causes spontaneous polarization, and dipoles build up. These dipoles have associated with them a strain which equilibriates in various domain configurations (Fig. 1). At room temperature, long exposure electron diffraction patterns reveal only weak superlattices about $\{h+\frac{1}{2},0,0\}$, $\{h+\frac{1}{2},k+\frac{1}{2},0\}$, and $\{h+\frac{3}{2},\ k+\frac{1}{2},0\}$ reflection. Cooling the samples down to $-170\,^{\circ}C$ reveals incommensurate satellite reflections about the above reciprocal lattice positions as observed in zone axis patterns $\langle 100\rangle$ and $\langle 211\rangle$, and shown in Figs. 2(a) and 2(b), respectively. First, we note the superlattice reflections marked "*F*-spot" which correspond to the long-range ordering of Co^{+2} and W^{+6} cations on the perovskite *B*-site sublattice to give a $2a_0\times 2a_0\times 2a_0$ ($a_0\approx 4.07$ Å) superlattice with an *F*

FIG. 1. Bright field micrograph of antiferroelectric phase at $-170\,^{\circ}C$ in $PbCo_{1/2}WO_3$.

centering. Second, we note the intensity distribution of the incommensurate satellite reflections across the electron diffraction patterns; the higher order $\{h+\frac{1}{2},0,0\}$, $\{h+\frac{1}{2},\ k+\frac{1}{2},0\}$, etc., satellite reflections show the stronger intensities. This could be due to the curvature of the Ewald sphere and the incommensurate satellites not lying exactly in the zeroth layer of the $\langle 001 \rangle$ reciprocal lattice, and also the displacive nature of the phase transition.[16] Third, the asymmetric spatial distribution of the satellites about the $\{h+\frac{1}{2},0,0\}$ and $\{h+\frac{1}{2},\ k+\frac{1}{2},0\}$ positions may be due to the low symmetries of monoclinic or triclinic as suggested by Tamura, Brixel, Filip'ev, and Fesenko.

Figure 3(a) shows a bright field (BF) image of the domain structure part and 3(b) shows a dark field image using the incommensurate diffraction spot [marked on Fig. 3(c)], revealing a discommensurate microstructure coexisting within the same region. From these micrographs we observe that the discommensurate microstructure is contained within the domains, and the domain walls (both from twin and inversion domains) act as barriers to the discommensuration. This may be due to a phase shift in the modulation at the domain walls.

Highly ordered $Pb(Sc_{1/2}Ta_{1/2})O_3$ also has incommensurate satellite spots about $\{h+\frac{1}{2},0,0\}$ and $\{h+\frac{1}{2},\ k+\frac{1}{2},0\}$ reciprocal lattice positions, and these vary with temperature within the ferroelectric phase. With sufficient B-site order (order domains ≥ 1000 Å) the incommensuration "locks in" below $-40\,^{\circ}C$, but this is very much determined by the degree of B-site order. Figure 4 shows the splitting of $\{h+\frac{1}{2},\ k+\frac{1}{2},0\}$ superlattice reflections at room temperature in a highly ordered $Pb(Sc_{1/2}Ta_{1/2})O_3$ single crystal; we also note the diffuse streaking about the matrix spots [see insert 4(b)]. The insert 4(a) shows the satellite splitting to be asymmetric; this again may point to a lower symmetry. Dark field imaging of the satellites reveals a discommensuration contrast with a periodicity $\cong 90$ Å, as observed in Fig. 5. The antiphase boundaries (APB's) caused by B-site ordering being 180° out-of-phase between neighboring ordering

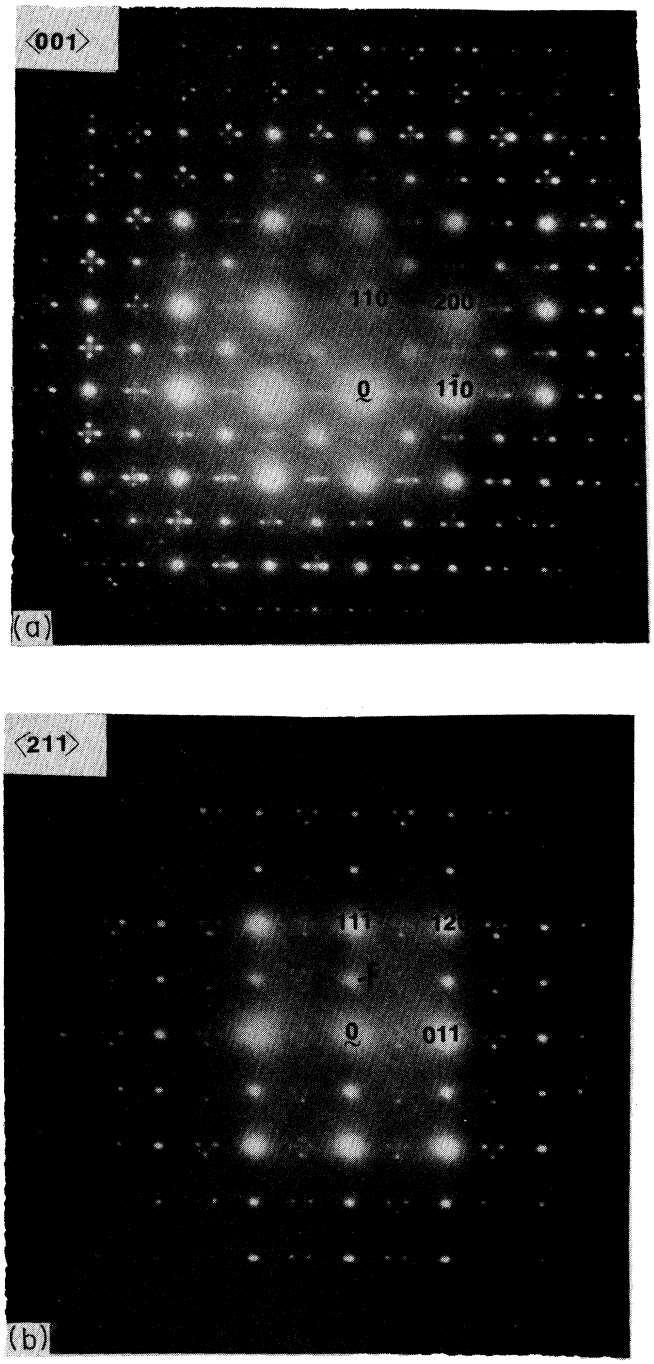

FIG. 2. Zone axis electron diffraction patterns from (a) $\langle 001 \rangle$ and (b) $\langle 211 \rangle$ at $-170\,^{\circ}C$ in $PbCo_{1/2}W_{1/2}O_3$.

domains does not act as barrier to the discommensuration microstructure, as observed in Fig. 6. However, the discommensuration microstructures are found to exist within ferroelectric domains in the $Pb(Sc_{1/2}Ta_{1/2})O_3$ and the ferroelectric domain walls act as barriers. The discommensurations disappear at lock in and only the ferroelectric domains remain.

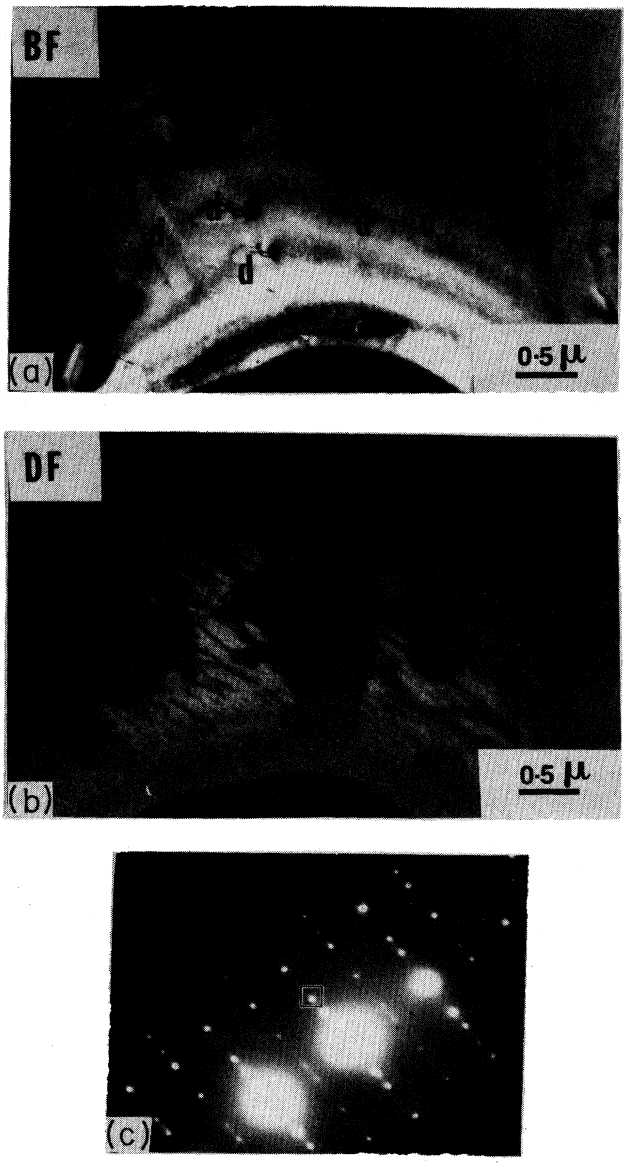

FIG. 3. (a) Bright field micrograph revealing the antiferroelectric domain structure in $PbCo_{1/2}W_{1/2}O_3$; (b) discommensurate microstructure from above area; (c) dark field image obtained using incommensurate satellite about the $\frac{1}{2}$ $\frac{1}{2}$ 0 position, at a temperature $\sim 170\,^{\circ}C$.

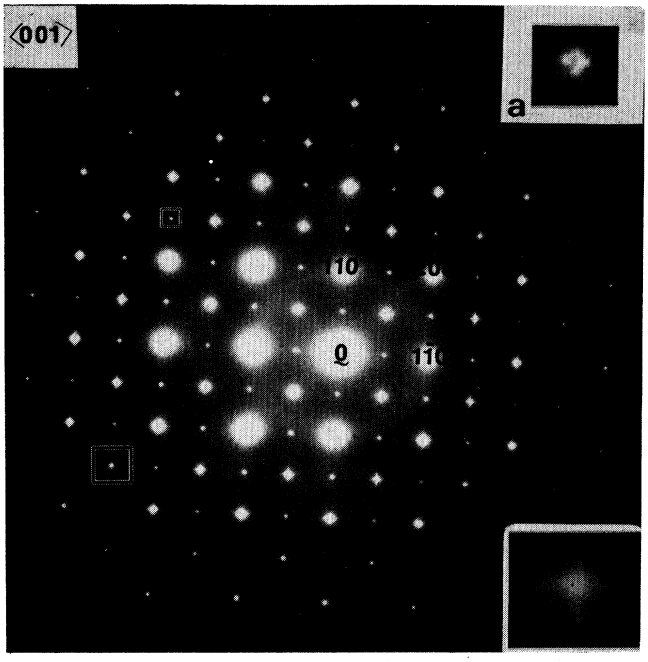

FIG. 4. Zone axis electron diffraction pattern from a highly ordered PST in the ferroelectric phase at room temperature.

DISCUSSION

The above-mentioned results point to the existence of incommensurate ferroelectric and antiferroelectric behavior within some of the $x = \frac{1}{2}$ highly ordered lead-based perovskites, e.g., $Pb(Sc_{1/2}Ta_{1/2})O_3$ and $Pb(Co_{1/2}W_{1/2})O_3$. Both of these perovskites show a direct interaction between the ferroelectric (antiferroelectric) domains and the discommensuration structures as suggested by the TEM studies. This implies a new type of ferroelectric-antiferroelectric incommensurate phase transition. To date, the most commonly observed behavior in ferroelectric incommensurate crystals is a prototype to an incommensurate phase through a second-order phase transition. The commensurate ferroelectric phase appears at a first-order phase transition.

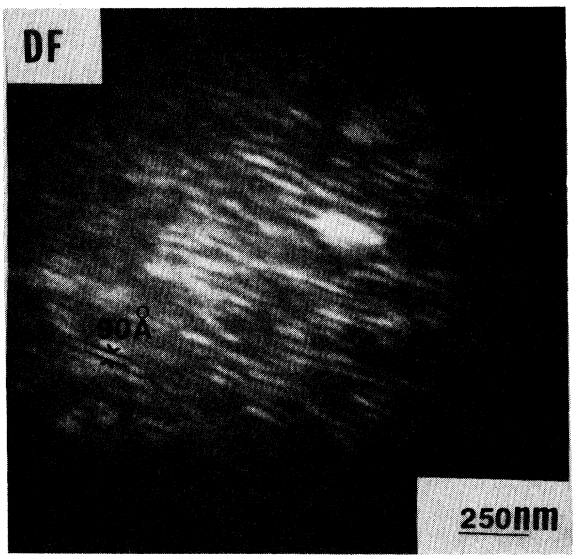

FIG. 5. Discommensuration structures found in highly ordered PST, obtained by dark field imaging two satellites about the $\frac{1}{2}$ $\frac{1}{2}$ 0 position, at room temperature.

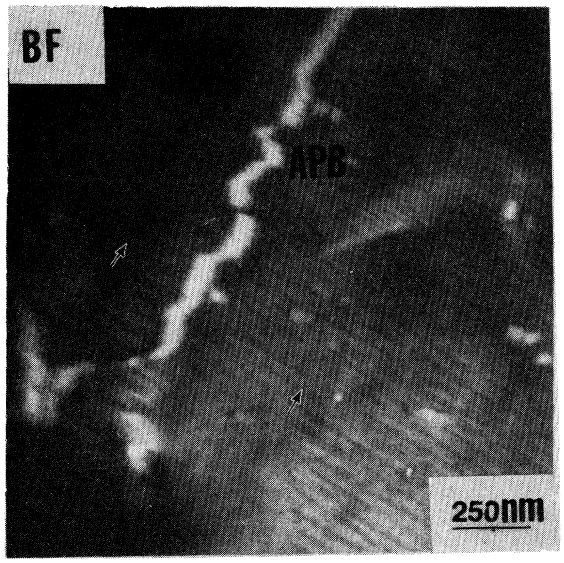

FIG. 6. Discommensuration structure showing no perturbation with the antiphase boundaries in PST.

Despite a number of studies on both $Pb(Sc_{1/2}Ta_{1/2})O_3$ and $Pb(Co_{1/2}W_{1/2})O_3$, no detailed structure determinations exist; it is hoped this study may stimulate such an undertaking. The $Pb(Sc_{1/2}Ta_{1/2})O_3$ has always been considered to be of rhombohedral symmetry from x-ray and optical studies at room temperatures, but the new superlattices and the asymmetric satellites point to a lower symmetry than previously expected. Generally, in ordinary lead-based perovskite ferroelectrics the cations displace relative to the anions in either ⟨001⟩ or ⟨111⟩ directions to give tetragonal or rhombohedral symmetry. However, at lower temperatures the dipole may turn away from the ⟨111⟩ direction to give symmetries lower than expected. Some of the confusing aspects from this preliminary study on the incommensurate structures are that although the *B*-site long-range order is a necessary requirement for the incommensurate phases, the discommensurations show no interaction with the antiphase boundaries. Also the new superlattices are on planes different from the *B*-site ordering [which is on {111} planes]. This points to a complex coupling between the *A*- and *B*-site sublattices, i.e., nearest-neighbor and next-neighbor interactions. Inequivalent dipole ordering (either parallel or antiparallel) might account for these new superlattices in the commensurate phase. If this is the case, the relative magnitudes of inequivalent antidipole ordering would make assigning a ferroelectric or an antiferroelectric nature to a given composition by just dielectric and basic x-ray characterization difficult. Clearly, a reexamination of the many ferroelectric and/or antiferroelectric phases with ordered *B*-site lead-based perovskites order must be undertaken with fuller characterization techniques.

CONCLUSIONS

Incommensurate antiferroelectric and ferroelectric phases are detected by cold-stage TEM studies on the perovskites $Pb(Co_{1/2}W_{1/2})O_3$ and $Pb(Sc_{1/2}Ta_{1/2})O_3$, respectively. A "lock-in" transition is found within the $Pb(Sc_{1/2}Ta_{1/2})O_3$ but the incommensurate to commensurate transition temperature is dependent on the degree of *B*-site order. The antiferroelectric and ferroelectric domains are found to be natural boundaries for the incommensuration, implying a strong coupling between the two phenomena.

[1]T. Shrout and A. Halliyal, Am. Ceram. Soc. Bull. **66**, 704 (1987).
[2]K. Uchino, Am. Ceram. Soc. Bull. **65**, 647 (1986).
[3]R. W. Whatmore, R. C. Osbond, and N. M. Shorrocks, Ferroelectrics **76**, 351 (1987).
[4]N. Setter and L. E. Cross, J. Appl. Phys. **51**, 4356 (1980).
[5]G. A. Smolenskii, J. Phys. Soc. Jpn. Suppl. **28**, 26 (1970).
[6]L. E. Cross, Ferroelectrics **76**, 241 (1987).
[7]C. A. Randall, D. J. Barber, and R. W. Whatmore, J. Microsc. **145**, 235 (1987).
[8]V. A. Bokov, S. A. Kizhaev, I. E. Myl'nikova, and A. G. Tutov, Fiz. Tverd. Tela (Leningrad) **6**, 3038 (1964) [Sov. Phys. Solid State **6**, 2419 (1965)].
[9]T. Hachiga, S. Fujimoto, and N. Yasuda, Jpn. J. Appl. Phys. Suppl. **24**, 239 (1985).
[10]W. Brixel, M. L. Werk, P. Fischer, W. Buhrer, J. P. Rivera, P. Tissot, and H. Schmid, Jpn. J. Appl. Phys. Suppl. **24**, 242 (1985).
[11]F. Maaroufi, P. Toledano, H. Schmid, W. Brixel, and W. Buhrer, Ferroelectrics **79**, 295 (1988).
[12]H. Tamura, Ferroelectrics **21**, 449 (1978).
[13]V. S. Filip'ev and E. G. Fesenko, Kristallografiya **9**, 293 (1964) [Sov. Phys.—Crystallog. **9**, 231 (1964)].
[14]N. Setter and L. E. Cross, J. Cryst. Growth **50**, 555 (1980).
[15]X. Y. Tamashpol'skii and Y. N. Venevtsev, Fiz. Tverd. Tela (Leningrad) **6**, 2998 (1965) [Sov. Phys. Solid State **6**, 2388 (1965)].
[16]J. W. Steeds, D. M. Bird, D. J. Eaglesham, S. McKernan, R. Vincent, and R. L. Withers, Ultramicroscopy **18**, 97 (1985).

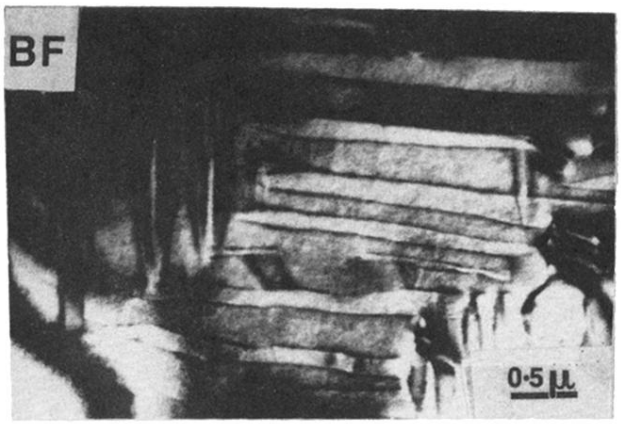

FIG. 1. Bright field micrograph of antiferroelectric phase at $-170\,^{\circ}C$ in $PbCo_{1/2}WO_3$.

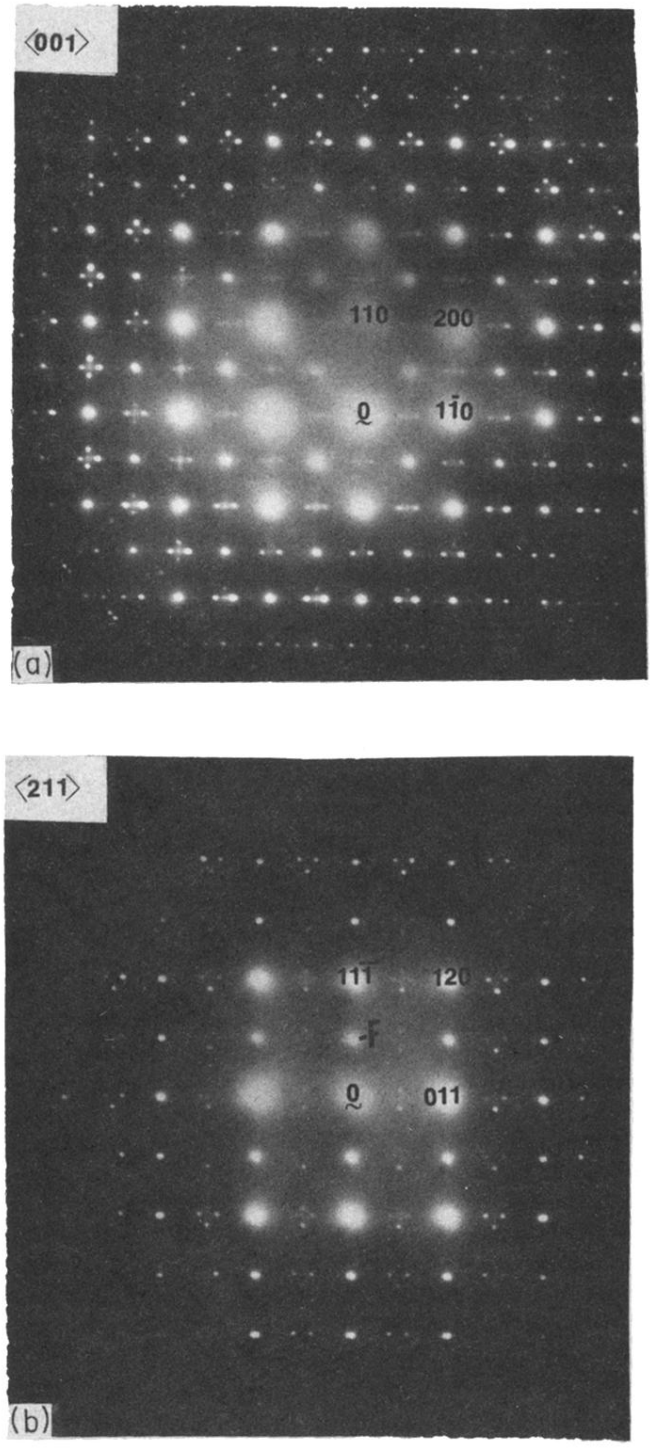

FIG. 2. Zone axis electron diffraction patterns from (a) ⟨001⟩ and (b) ⟨211⟩ at −170 °C in $PbCo_{1/2}W_{1/2}O_3$.

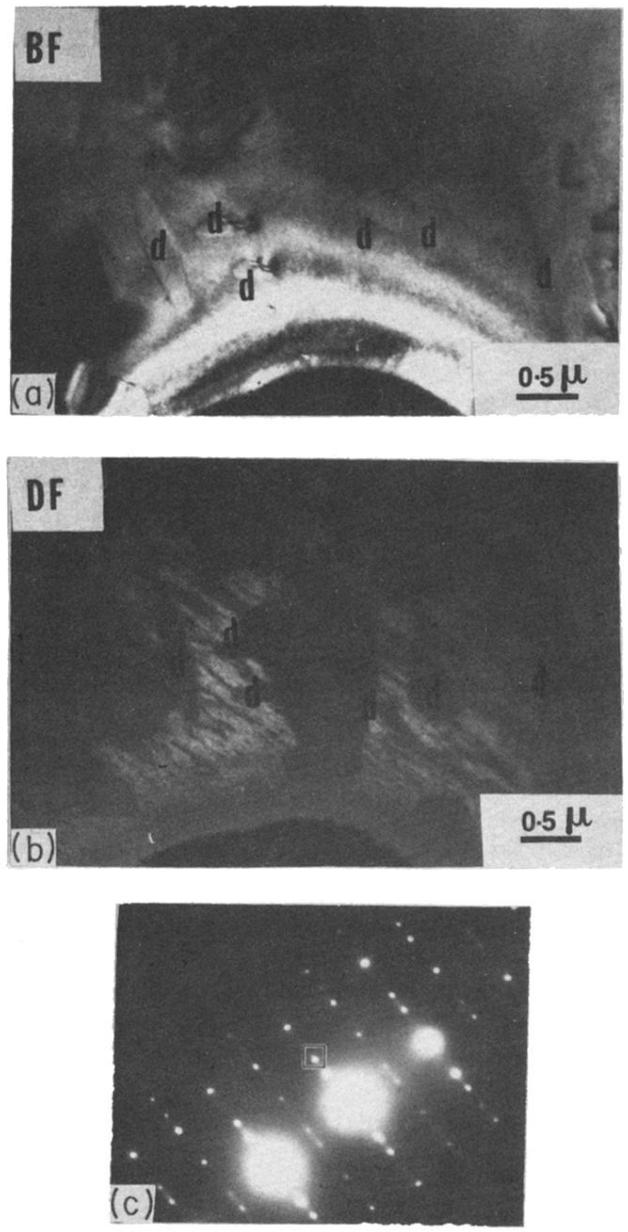

FIG. 3. (a) Bright field micrograph revealing the antiferroelectric domain structure in $PbCo_{1/2}W_{1/2}O_3$; (b) discommensurate microstructure from above area; (c) dark field image obtained using incommensurate satellite about the $\frac{1}{2}$ $\frac{1}{2}$ 0 position, at a temperature $\sim 170\,^{\circ}C$.

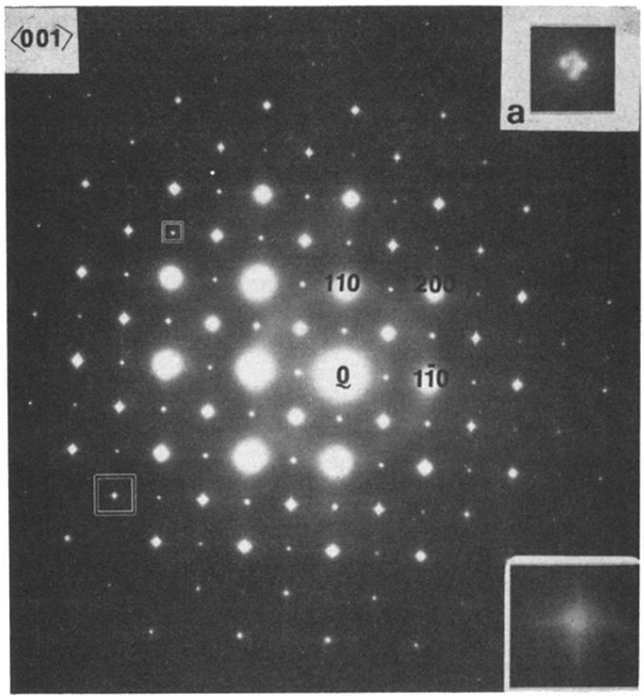

FIG. 4. Zone axis electron diffraction pattern from a highly ordered PST in the ferroelectric phase at room temperature.

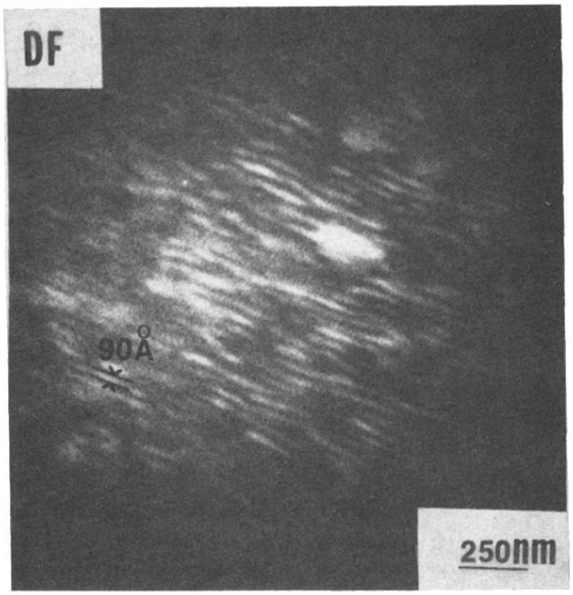

FIG. 5. Discommensuration structures found in highly ordered PST, obtained by dark field imaging two satellites about the $\frac{1}{2}\ \frac{1}{2}\ 0$ position, at room temperature.

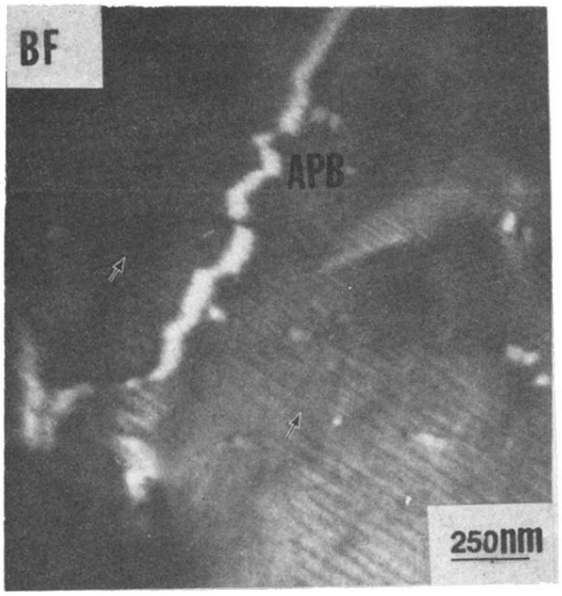

FIG. 6. Discommensuration structure showing no perturbation with the antiphase boundaries in PST.